JOURNAL OF GUIDANCE, CONTROL, AND DYNAMICS
Vol. 27, No. 5, September–October 2004

Control of a Rotating Variable-Length Tethered System

Mischa Kim* and Christopher D. Hall†
Virginia Polytechnic Institute and State University, Blacksburg, Virginia 24061

Techniques are developed and illustrated to control the motion of a tethered satellite system (TSS) comprising n point masses and interconnected arbitrarily by m idealized tethers. In particular, the control problem of a triangular and symmetrical TSS with $n = 3$ point masses and $m = 3$ tethers is discussed. The equations of motion are derived by the use of Lagrange's equations. Several mission scenarios for a proposed NASA mission that consider the operation of an infrared telescope are introduced and asymptotic tracking laws based on input-state feedback linearization are developed. The effects of smoothness and nonsmoothness of desired mission trajectories on control performance are discussed. It is shown that required thrust levels can be significantly decreased by the use of additional tether length control to keep the TSS in a state corresponding to an instantaneous relative equilibrium at any point in time during the mission. In the final section, a mathematical model is proposed for the total required control impulse to facilitate a trade study that discusses the effects of the individual system parameters on the control input.

Introduction

OVER the past three decades, a variety of concepts have been proposed for space exploration that use tethered satellite systems (TSS). These concepts include scientific experiments in the microgravity environment, upper atmospheric research, cargo transfer between orbiting bodies, generation of electricity, and deep space observation.[1–3] Numerous missions have already been launched to verify the tethered system concept for space application. Important milestones include retrieval of a tether in space (TSS-1, 1992), successful deployment of a 20-km tether in space (SEDS-1, 1993), closed-loop control of a tether deployment (SEDS-2, 1994), and operation of an electrodynamic tether used in both power and thrust mode (PMG, 1993).[4,5] The idea of interconnection of spacecraft by means of lightweight deployable tethers has also been proven to be particularly attractive for space observations for various reasons. Variable-baseline interferometric observations can be achieved by a carefully controlled deployment/retrieval procedure of the tethers. In addition, the observational plane can be densely covered by spinning the tethered system. Last, the high levels of propellant consumption demanded by separated spacecraft in formation can be dramatically reduced by tension control of the interconnecting tethers.

The paper is organized as follows: To begin, a brief description of the science mission that motivated this study is presented. In the following section some relevant papers and articles on the dynamics and control of TSS are presented. Subsequently, the system model is introduced and the motion equations are derived. Relative equilibria are identified and other possible mission scenarios are presented. Control performance that use feedback linearization is validated, with consideration given to the different mission scenarios. Finally, we present a mathematical model to estimate the total required control impulse to complete a mission. This model considers the effects of the individual system parameters and is shown to compare well with numerical simulation results.

Received 18 June 2003; revision received 16 January 2004; accepted for publication 26 January 2004.

*Graduate Assistant, Aerospace and Ocean Engineering; mischa@vt.edu. Student Member AIAA.

†Professor, Aerospace and Ocean Engineering; cdhall@vt.edu. Associate Fellow AIAA.

SPECS Mission Concept

NASA's future Earth and space science missions involve formation flight of multiple coordinated spacecraft. Several space science missions include distributed instruments, large-phased arrays of lightweight reflectors, and long variable baseline space interferometers. An array of collectors and combiner spacecraft will form variable-baseline space interferometers for a variety of science missions such as the submillimeter probe of the evolution of cosmic structure (SPECS).[6] This particular mission concept was initiated by a NASA science team and proposes a 1-km baseline submillimeter interferometer ($\lambda \approx 40 - 500\ \mu$m). It comprises possibly as few as three 3–4-m-diam mirrors and rotates about the primary optical axis collecting (0.03–0.0025 eV) photons, which are then preprocessed by a central beam collector. Because the operation of such systems in any kind of Earth orbit is not feasible due to extensive fuel consumption and unsatisfactory photon yield, the second Lagrangian point in the sun–Earth system L_2 was chosen as the operational environment. The SPECS spacecraft formation is intended to be placed in a halo orbit about this libration point.[7]

Literature Review

Researchers have studied the complex dynamics of TSS using a variety of models. From the initial studies, where tethers were modeled to be perfectly flexible and inextensible, attention was shifted toward more realistic models accounting for tether mass, elasticity, and flexibility.

The dynamics and control problems associated with an Earth-orbiting, symmetrical, and triangular TSS were studied by DeCou.[8] He derived a control strategy assuming the entire system to be a rigid body in the presence of gravity gradient disturbances. The author showed that thrust and fuel levels are within state of the art for a 10-km baseline dumbbell-like interferometer operating in synchronous orbit. DeCou also introduced a method of damping tether vibrations using linear offset control. In another paper DeCou[9] studied the static shape of such TSS, assuming finite mass density of the tethers and that the tethers were under the influence of the centrifugal forces caused by the rotation of the system. Misra[10] investigated equilibrium configurations and stability characteristics of a three-body TSS whose center of mass moves in a circular orbit around the Earth. For his analysis, the tethers were assumed to have negligible mass and to be inextensible and rigid. In an earlier article, Misra et al.[11] studied the attitude dynamics of a system modeled as an ideal double pendulum on a circular orbit. They considered constant as well as variable tether length dynamics simulations. For the constant length cases, they studied equilibrium configurations and small motion around these configurations. Misra and Modi[12] investigated the dynamics of an ideal N-body TSS and developed

linear control laws for in- and out-of-plane motions to control librational dynamics in the neighborhood of stable vertical equilibrium configuration in a circular orbit. The equations of motion of an N-body TSS with flexible tethers using a continuum model were derived by Keshmiri and Misra[13] for dynamics simulations. The motion equations were linearized for control and stability analysis purposes. Librational, as well as longitudinal and transverse elastic frequencies of several multibody systems were obtained. Misra et al.[14] considered the dynamics of a dumbbell TSS in the vicinity of the Earth–moon Lagrangian points. Equilibrium configurations of the system near the libration points were determined, and librational frequencies about the stable configurations were calculated. Also, an in-depth analysis of the coupled motion of the center of mass and the tether libration was carried out for the dynamics near the translunar Lagrangian point. Farquhar analyzed the positional stability of the ideal dumbbell TSS located in the vicinity of a collinear Lagrangian point (see Ref. 15). The mass of the tethers was assumed to be negligible, and also the tension in the tethers was assumed to always be present. He showed that stability can be achieved by the use of a linear control law for the tether length. Farquhar also investigated the control of cable-connected satellites via range and range rate at the collinear Lagrange points (see Ref. 16). Farquhar's work built on an earlier paper by Colombo,[17] who suggested the stabilization of satellites in Halo orbits about the "inferior conjunction points" in the Earth–moon system via thrusters or a solar sail.

Extensive research has addressed basic TSS dynamics and control problems, whereas little attention has been paid to the controlled motion of a complex TSS in orbits around the second Lagrangian point in the sun–Earth system. This paper is a first step to gather a thorough understanding of the dynamics of such systems for future deep-space exploration. In the following section, the system model is introduced for a TSS comprising n point masses and m tethers.

System Model and Equations of Motion

Equations of motions (EOM) of the system are formulated by the use of the system description developed in Ref. 18. The mechanical system considered is shown in Fig. 1. It comprises a system of n point masses interconnected arbitrarily by m idealized tethers. The tethers are assumed to be massless and extensible, capable of exerting force only along the straight-line connecting the respective masses. Also, the tethers do not support compression or any components of shear forces or bending moments and are, therefore, assumed to be perfectly flexible. The constitutive character for the tethers is taken as viscoelastic, which allows intrinsic energy dissipation. Because the system is ultimately being operated at the second Lagrangian point L_2 in the sun–Earth system, gravitational and other environmental forces are assumed to be negligible, but are readily incorporated into the model if necessary.

The EOM are derived by the use of Lagrange's equations defined in a prescribed motion reference frame $\mathcal{F}_\mathcal{P}$, rather than in an inertial reference frame $\mathcal{F}_\mathcal{I}$. Cylindrical coordinates relative to $\mathcal{F}_\mathcal{P}$ are chosen to describe the position of the point masses. As shown in Fig. 1, r_i, θ_i, and z_i are the radial distance in the $\boldsymbol{e}_x\boldsymbol{e}_y$ plane, the angle between the $\boldsymbol{e}_x$ axis and the projection of the position vector $\boldsymbol{q}_i$ onto the $\boldsymbol{e}_x\boldsymbol{e}_y$ plane, and the axial distance in the $\boldsymbol{e}_z$ direction of the point mass m_i, respectively. The formulation is generalized by the addition of rheonomic constraints to allow for specification of any or all of the degrees of freedom. The motion equations for the controlled system are

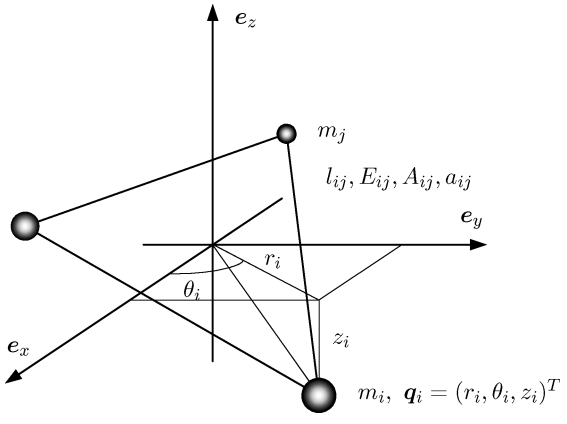

Fig. 1 System model in cylindrical coordinates.

$$\boldsymbol{M}_i\ddot{\boldsymbol{q}}_i = \boldsymbol{Q}_i^{(e)} + \boldsymbol{N}_i + \boldsymbol{S}_i + \boldsymbol{U}_i, \qquad i = 1, 2, \ldots, n \tag{1}$$

where

$$\boldsymbol{M}_i = m_i \begin{bmatrix} 1 & 0 & 0 \\ 0 & r_i^2 & 0 \\ 0 & 0 & 1 \end{bmatrix}, \qquad \boldsymbol{q}_i = \begin{pmatrix} r_i \\ \theta_i \\ z_i \end{pmatrix}$$

$$\boldsymbol{Q}_i^{(e)} = \begin{pmatrix} F_{ri} \\ r_i F_{\theta i} \\ F_{zi} \end{pmatrix}, \qquad \boldsymbol{S}_i = \boldsymbol{Q}_i^{(i)} \tag{2}$$

In Eqs. (1), $\boldsymbol{M}_i$, $\boldsymbol{q}_i$, $\boldsymbol{Q}_i^{(e)}$, $\boldsymbol{N}_i$, $\boldsymbol{S}_i$, and $\boldsymbol{U}_i$ are the mass matrix, the vector of generalized coordinates, and the vectors of external, coupling, spring (or internal), and control forces for the ith point mass, respectively. By definition of the vector of generalized coordinate vectors for the system as $\boldsymbol{q} = (\boldsymbol{q}_1^T, \boldsymbol{q}_2^T, \ldots, \boldsymbol{q}_{n-1}^T, \boldsymbol{q}_n^T)^T$ Eqs. (1) can be combined to yield

$$\boldsymbol{M}\ddot{\boldsymbol{q}} = \boldsymbol{Q}^{(e)} + \boldsymbol{N} + \boldsymbol{S} + \boldsymbol{U} \tag{3}$$

where $\boldsymbol{M}$, $\boldsymbol{Q}^{(e)}$, $\boldsymbol{N}$, $\boldsymbol{S}$, and $\boldsymbol{U}$ are defined appropriately. Notice that Eqs. (3) are readily integrated after being transformed to a set of $2 \times 3n$ first-order equations; that is, by the definition $\boldsymbol{x} = (\boldsymbol{q}, \dot{\boldsymbol{q}})^T$, Eqs. (3) can be written in compact form as

$$\dot{\boldsymbol{x}} = \boldsymbol{f}(\boldsymbol{x}) + \boldsymbol{G}(\boldsymbol{x})\boldsymbol{u}, \qquad \boldsymbol{f}(\boldsymbol{x}) = \begin{pmatrix} \dot{\boldsymbol{q}} \\ \boldsymbol{M}^{-1}(\boldsymbol{Q}^{(e)} + \boldsymbol{N} + \boldsymbol{S}) \end{pmatrix} \tag{4}$$

and $\boldsymbol{G}(\boldsymbol{x}) = (\boldsymbol{g}_1, \ldots, \boldsymbol{g}_p)$ and $\boldsymbol{u}$ are defined obviously. For the subsequent analysis, a TSS comprising $n = 3$ point masses and $m = 3$ tethers is considered, as shown in Fig. 1.

Relative Equilibria

The spring forces appearing in Eqs. (1) can be written as

$$\boldsymbol{S}_i = \sum_{\substack{j=1 \\ j \neq i}}^{n=3} \frac{f_{ij}}{l_{ij}} \begin{pmatrix} \sigma_{ij} \\ \tau_{ij} \\ \zeta_{ij} \end{pmatrix} \tag{5}$$

where we have introduced the quantities

$$\sigma_{ij} = r_j \cos(\theta_j - \theta_i) - r_i, \qquad \tau_{ij} = r_i r_j \sin(\theta_j - \theta_i)$$

$$\zeta_{ij} = z_j - z_i \tag{6}$$

Additionally, in the rotating reference frame $\mathcal{F}_\mathcal{P}$, the relative equilibrium motion satisfies $\dot{\boldsymbol{x}}^e = \boldsymbol{f}(\boldsymbol{x}^e) = \boldsymbol{0}$, where the superscript denotes the relative equilibrium state. Under the assumption of a perfectly symmetrical TSS, it is sufficient to analyze either of the subsystems described by Eqs. (1). Temporarily dropping the point mass subscript notation and noting that $|\theta_j - \theta_i| = 2\pi/3$, we find three conditions for each of the three point masses of the form

$$r^e = \text{constant} \tag{7}$$

$$\dot{\theta}^e(r^e) = \sqrt{\frac{\sqrt{3}EA\left(\sqrt{3}r^e - d\right)}{mr^e d}}, \qquad l^e = \sqrt{3}r^e \tag{8}$$

$$z^e = \text{constant} \tag{9}$$

Therefore, the relative equilibrium angular velocity for the TSS is

$$\dot{\theta}^e(l^e) = \sqrt{\frac{3EA(l^e - d)}{ml^e d}} \tag{10}$$

which shows that the rotating TSS has to be under tension ($l^e > d$).

Mission Scenarios for SPECS

Three different mission scenarios are used to validate the control law developed in the following section. The first scenario deals with the control of the TSS to a specific relative equilibrium. Mission scenarios two and three describe trajectory designs that are relevant for the SPECS mission. To decrease overall thrust levels, refinements to the control laws are introduced that include additional tether length control.

A. Mission Scenario 1: Stabilization of a Relative Equilibrium Motion

The first mission scenario considers the stabilization of a particular relative equilibrium motion of the TSS. This case is of importance for those phases during the sequence of observations when the satellite formation needs to be reoriented to point at specific targets of interest. When Eqs. (7–9) are used, the desired trajectories $\boldsymbol{y}_{i,d}$ for the point masses m_i are

$$\boldsymbol{y}_{i,d} = (r_{i,d}, \theta_{i,d}, z_{i,d})^T = \left(r^e, t\dot{\theta}^e + (i-1)\theta_\Delta, z^e\right)^T \qquad i = 1, 2, 3 \tag{11}$$

where $\theta_\Delta = 2\pi/3$ and with appropriately chosen initial conditions. Figure 2 shows a typical initial conditions perturbation response.

B. Mission Scenario 2: Simple Tether Deployment/Retrieval Mission

The aforementioned mission scenario can be extended to include a tether deployment/retrieval procedure that allows the system to (partially or fully) cover the observational plane. Figure 3 shows the time history of the desired trajectory and the trace of one of the point masses for the proposed mission. Note that the angular velocity of the system is chosen to be constant during the entire mission. Also, the time rate of change of the radial distance of the point masses is assumed to be constant during tether deployment/retrieval. Obviously, depending on the ratio (radial deployment/retrieval rate):(system

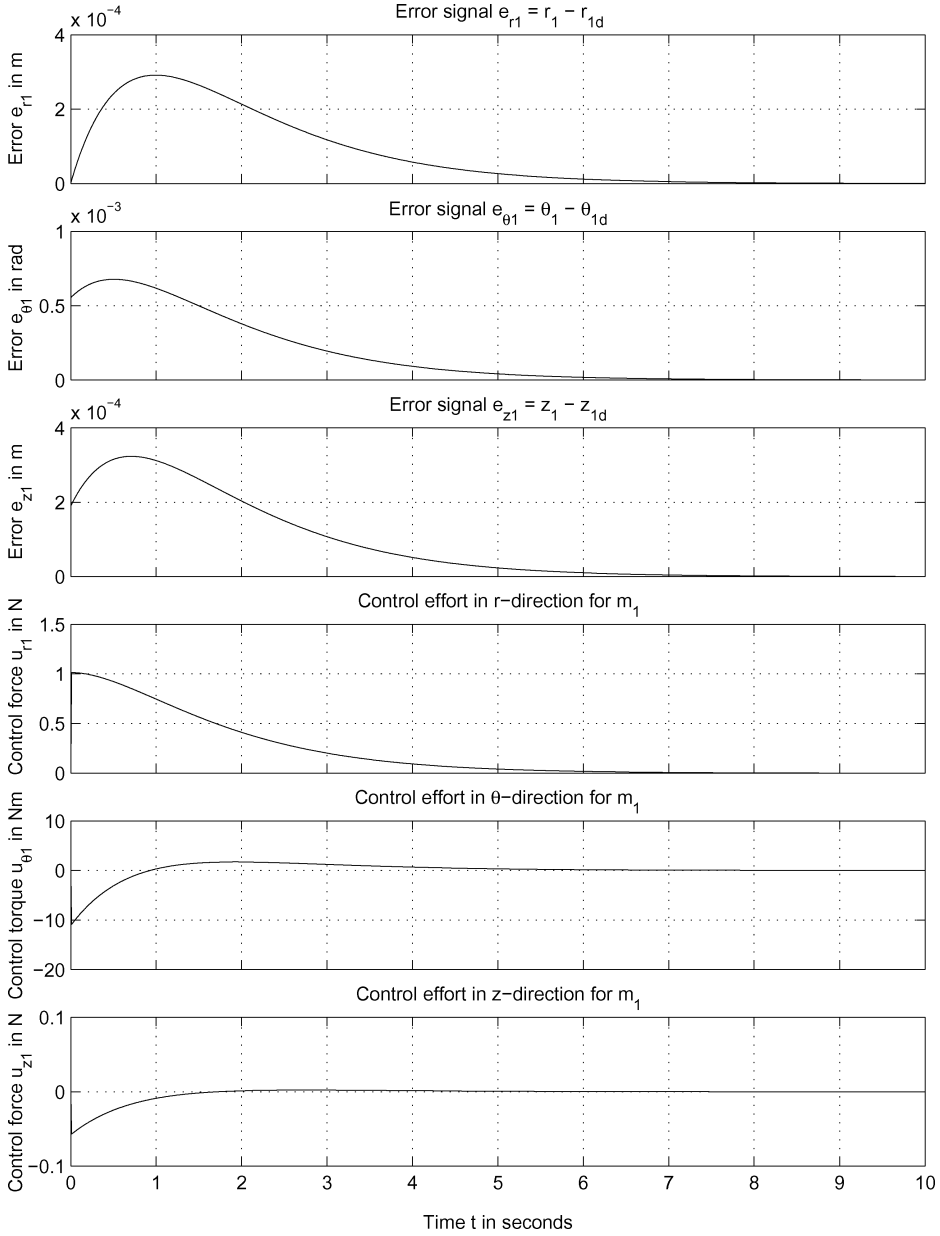

Fig. 2 Initial conditions perturbation response.

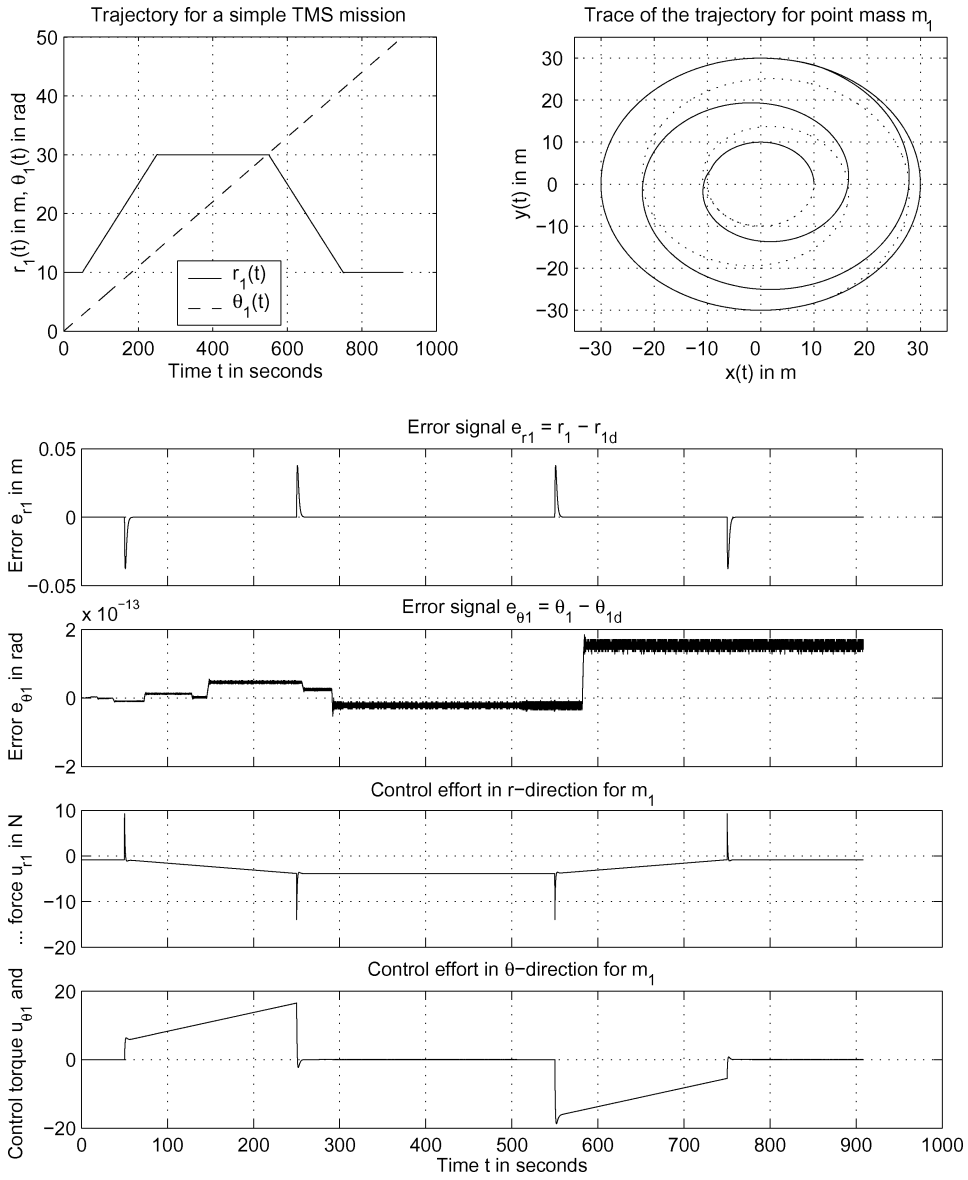

Fig. 3 Trajectory, output error, and control vector time histories for mission scenario 2.

angular velocity), partial or full coverage of the observational plane is obtained for a given mirror diameter.

For this mission scenario, different prescribed tether length control laws can be formulated. Two tether length control laws are chosen for comparison: The first assumes a simple linear relationship between the radial distance of the point masses and the tether length, whereas the second prescribes a tether length history such as to keep the TSS in a relative equilibrium at any point in time during the mission.

C. Mission Scenario 3: SPECS Relevant Mission Scenario

Further refinements to possible mission trajectories can be made by the requirement that the mirrors to cover the observational plane use a more efficient pattern like an Archimedes spiral, which is described in polar coordinates by $r = a\theta$, where a is an arbitrary constant. For this particular mission scenario, an additional scientifically motivated constraint is formulated to define a specific trajectory unambiguously. In particular, we require that the instantaneous tangential velocity of each of the three point masses never exceeds a maximal value $v_{\max}$. Figure 4 shows an example of such a mission trajectory. Temporarily dropping the subscript notation due to system symmetry, the three positional constraints for the TSS are

$$\mathrm{d}r = (3D/2\pi)\,\mathrm{d}\theta, \qquad r\dot{\theta} = v_{\max}, \quad \text{and} \quad z = \text{constant} \tag{12}$$

where D is the mirror diameter. These constraints can be combined to yield

$$r\dot{r} = \frac{1}{2}\frac{\mathrm{d}}{\mathrm{d}t}(r^2) = \frac{3Dv_{\max}}{2\pi} =: \alpha = \text{constant} \tag{13}$$

Therefore, the radial function has to be of the form $r = c_1\sqrt{(t + c_2)}$. Substitution of this ansatz function into equations (12) and (13) eventually results in

$$r_d = \sqrt{r_{0_+}^2 + 2\alpha t}, \qquad \theta_d = \theta_{0_+} - (v_{\max}/\alpha)\left(r_{0_+} - \sqrt{r_{0_+}^2 + 2\alpha t}\right)$$
$$z_d = z_{0_+} \tag{14}$$

where r_{0_+}, θ_{0_+}, and z_{0_+} are the initial conditions for deployment. Equations (14) describe the time history of each of the point masses during tether deployment. A similar analysis for the retrieval procedure eventually yields for the desired deployment/retrieval trajectories

$$r_{i,d} = \sqrt{r_{0_\pm}^2 \pm 2\alpha t}$$

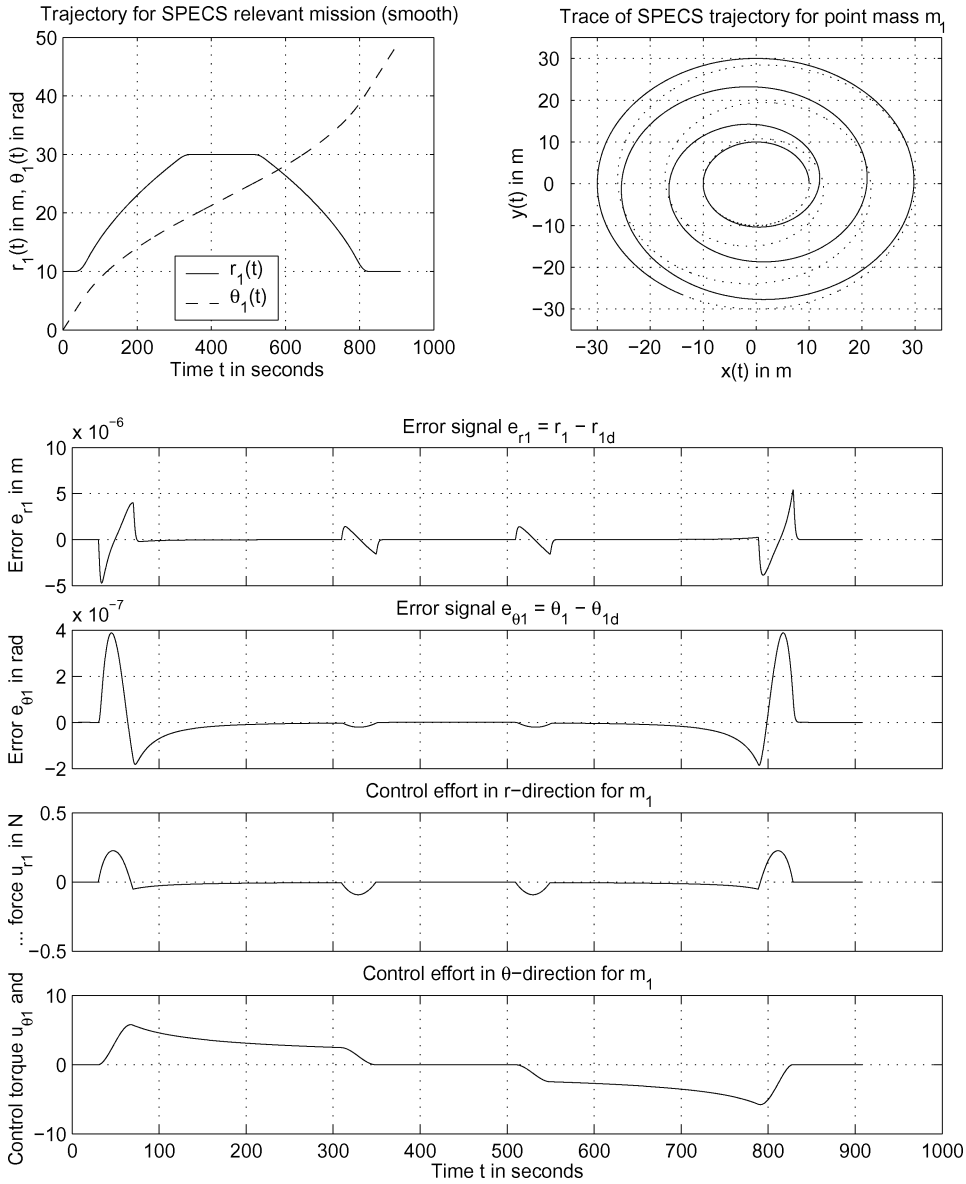

Fig. 4 Smooth trajectory, output error, and control vector time histories for mission scenario 3.

$$\theta_{i,d} = \theta_{0_\pm} + (i-1)\theta_\Delta - (v_{\max}/\alpha)\Big(\pm r_{0_\pm} \mp \sqrt{r_{0_\pm}^2 \pm 2\alpha t}\Big) \qquad i = 1, 2, 3$$

$$z_{i,d} = z_{0_\pm} \tag{15}$$

In Eqs. (15), the upper signs hold for tether deployment and the lower signs hold for tether retrieval phases. Initial conditions for both procedures are denoted by $\boldsymbol{q}_{0_\pm} = (r_{0_\pm}, \theta_{0_\pm}, z_{0_\pm})^T$, where the plus/minus sign indicates tether deployment/retrieval.

Improvements to the SPECS Trajectory: Introduction of Smoothing Functions

Discontinuities in the functions describing the desired trajectory result in undesirable discontinuities in requested controls; thus, we introduce smoothing functions into the desired trajectory during critical periods of time. For the SPECS trajectory developed in the preceding section, this matter is complicated by the fact that the radial and angular components of the trajectory are not independent ($r\dot{\theta} = v_{\max}$). Integration of an ansatz function of the form

$$\ddot{\theta}_{i,d} = C_1\big(t - t_s^o\big)^3 + C_2\big(t - t_s^o\big)^2 + C_3\big(t - t_s^o\big), \qquad i = 1, 2, 3 \tag{16}$$

yields algebraic expressions for $\ddot{\theta}_{i,d}$ and $\dot{\theta}_{i,d}$. In Eqs. (16), t_s^o denotes the starting time of the smoothing process. Constants C_i are derived to formulate appropriate boundary transition conditions at the endpoints of the smoothing interval at $t = t_s^o$ and $t = t_s^f$. For example, for the initial segment of the SPECS trajectory, where the system changes from a steady-spin motion into the tether deployment phase, these conditions yield

$$t = t_s^o: \qquad \dot{\theta}_{i,d} = v_{\max}\big/r_{0_+}, \qquad \ddot{\theta}_{i,d} = 0, \qquad \dddot{\theta}_{i,d} = 0$$

$$t = t_s^f: \qquad \dot{\theta}_{i,d} = v_{\max}/r_\star, \qquad \ddot{\theta}_{i,d} = -\alpha v_{\max}\big/r_\star^3$$

$$\dddot{\theta}_{i,d} = 3\alpha^2 v_{\max}\big/r_\star^5 \tag{17}$$

where $r_\star = \sqrt{[r_{0_+}^2 + 2\alpha(t_s^f - t^\star)]}$ and where $t^\star$ denotes the starting time of the tether deployment phase for the nonsmooth SPECS trajectory. Coefficients C_1, C_2, and C_3 are uniquely determined by the three conditions at time $t = t_s^f$. Note that the latter two conditions at $t = t_s^o$ are trivially satisfied, whereas the first condition fixes an additional integration constant C_4 that appears in the analytic expression for $\dot{\theta}_{i,d}$. Consideration of the constraint $r\dot{\theta} = v_{\max}$ yields functions $r_{i,d}$, $\dot{r}_{i,d}$, and $\ddot{r}_{i,d}$. Note that the special choice of $\dddot{\theta}_{i,d}$ guarantees that 1) $\ddot{r}_{i,d} = \ddot{r}_{i,d}(\dot{\theta}_{i,d}, \ddot{\theta}_{i,d}, \dddot{\theta}_{i,d})$ is continuous, and, therefore,

$\dot{r}_{i,d}$, $r_{i,d}$ is smooth, and 2) $\dot{\theta}_{i,d} \neq 0$, and, therefore, $r_{i,d}$ is bounded for $t \in [t_s^o, t_s^f]$.

In the next section, the tools necessary to develop a nonlinear feedback controller based on input-state feedback linearization are introduced.

Control Law Development

In this section, we discuss controllers based on feedback linearization.[19,20] Feedback linearization guarantees suboptimal performance only, which may result in increased propellant consumption in general. However, implementing the more complex tether length control law described by Eq. (10), we obtain significantly improved performance results. A more serious drawback of an observer-based control approach is that an accurate physical model of the dynamic system is required to guarantee asymptotic stability. Although the mathematical structure of the system is usually well defined, the physical parameters are often not precisely known. Additionally, the cost of the implementation of a controller based on input-state feedback typically includes the cost of motion sensors, which, in turn, results in elevated sensor count. Adaptive output-feedback controllers utilizing a velocity-generated filter and an estimator for system parameters offer an elegant solution to the problem.[21]

For this analysis, the positions of the point masses m_i are chosen as outputs; that is, $\boldsymbol{y}_i \equiv \boldsymbol{q}_i = (r_i, \theta_i, z_i)^T$, $i = 1, 2, 3$. Also, due to the particular choice of control inputs in Eqs. (1), it is straightforward to show that the system is completely controllable.

Regulator Design Using Input-State Feedback Linearization

The investigated system is a so-called square system (number of inputs equals the number of outputs) of the form

$$\dot{\boldsymbol{x}} = \boldsymbol{f}(\boldsymbol{x}) + \boldsymbol{G}(\boldsymbol{x})\boldsymbol{u}, \qquad \boldsymbol{y} = \boldsymbol{h}(\boldsymbol{x}) \tag{18}$$

where $\boldsymbol{x} \in \mathbb{R}^N$, $\boldsymbol{u} = (\boldsymbol{u}_1^T, \ldots, \boldsymbol{u}_p^T)^T \in \mathbb{R}^P$, $\boldsymbol{y} = (\boldsymbol{y}_1^T, \ldots, \boldsymbol{y}_p^T)^T \in \mathbb{R}^P$, $\boldsymbol{f}$ and $\boldsymbol{g}_j$ are assumed to be smooth vector fields, and h_i is assumed to be smooth functions in some domain D_0. Note that, for the TSS, $N = 2 \times 3n = 18$ and $P = 3n = 9$.

Recall that with $\boldsymbol{x}_i = (r_i, \theta_i, z_i, \dot{r}_i, \dot{\theta}_i, \dot{z}_i)^T = (\boldsymbol{q}_i, \dot{\boldsymbol{q}}_i)^T$, and due to the symmetry of the system, the equations of motions of the TSS can be analyzed as three subsystems, each of which describes the dynamics of one of the point masses. The controlled motion equations are

$$\dot{\boldsymbol{x}}_i = \begin{pmatrix} \dot{\boldsymbol{q}}_i \\ \boldsymbol{M}_i^{-1}\left(\boldsymbol{Q}_i^{(e)} + \boldsymbol{N}_i + \boldsymbol{S}_i + \boldsymbol{U}_i\right) \end{pmatrix}, \qquad i = 1, 2, 3 \tag{19}$$

where $\boldsymbol{U}_i$, $i = 1, 2, 3$ are the control inputs. Note that, due to the particular choice of inputs and outputs, the system is already in normal form.[22]

The design of the controller for an asymptotic tracking problem is straightforward because the inputs directly govern the motion of the outputs. That is, given a dynamic system described by Eqs. (18) and a desired trajectory $\boldsymbol{y}_d$, find a control law for the input $\boldsymbol{u}$ such that, starting from any initial state in a domain D_0, the tracking error vector $\boldsymbol{e} = \boldsymbol{y} - \boldsymbol{y}_d$ goes to zero, whereas the state remains bounded. For a thorough analysis on asymptotic tracking for multi-input/multi-output (MIMO) systems, we refer to Refs. 20 and 22.

Note that the smoothness condition stated earlier is not necessarily strictly fulfilled at all times during a mission due to the discontinuities in the tether elastic forces. However, even though these critical phases during tether deployment/retrieval are likely to occur in a real observation, they are by all means rare events and are, therefore, assumed to be negligible for the present analysis. Also, a more complex coupled control law for the point masses and the tether tension/length should be capable of keeping the system under tension during an entire mission.

Gain Selection for the Linear Controller

Asymptotic tracking via feedback linearization decouples the individual coordinate directions, and a set of structurally similar equations are obtained. It is, therefore, sufficient to analyze only one of these equations. When the subscript notation is temporarily dropped and notice is taken that only time derivatives up to an order of $\rho = 2$ are involved, the linear system can be written as

$$\ddot{e} + a\dot{e} + be = 0 \tag{20}$$

A powerful tool for linear control system design is the root-locus method to obtain the system root locations relative to a single parameter. One way to identify this particular parameter in a second-order system represented by Eq. (20) is to rewrite its characteristic polynomial as

$$s^2 + as + b = s^2 + a(s + b/a) = 0 \qquad \text{or} \qquad s^2 + K(s + c) = 0 \tag{21}$$

where K and c are chosen obviously. For $a > 0$ and $b > 0$, the roots of this characteristic equation are all strictly in the left-half plane, and the system is asymptotically stable. Figure 4a shows the corresponding root-locus plot for varying K. The roots of the characteristic equation are

$$s_{1,2} = \left(-a \pm \sqrt{a^2 - 4b}\right)/2 \tag{22}$$

Aiming for a critically damped system, we note that the roots and the parameter K for this case are

$$s_{1,2}^c = -a/2 = -2c, \qquad K^c = 4c \tag{23}$$

In Fig. 5a, this point is found at the intersection of the circle with the real axis in the left-half plane. Note that the size of the circle depends on the ratio $c = b/a$, whereas the exact location of the roots are a function of a only once c is fixed. It is, therefore, reasonable to choose $K(=a)$ as the representative parameter because the size of the circle can be chosen as a function of system performance criteria such as time-domain specifications for a step response (Figs. 5b and 5c). For second-order systems, a standard approach to describe the transient response to a step function is to specify parameters such as rise time t_r, settling time t_s, and overshoot M_p. These parameters are then translated into corresponding parameters in the s-plane by the use of[23]

$$\omega_n \approx 1.8/t_r, \qquad \sigma \approx 4.6/t_s, \qquad \varphi = \sin^{-1}\zeta \tag{24}$$

where $\zeta = \sqrt{[\alpha/(1+\alpha)]}$ and $\alpha = (\ell_n M_p/\pi)^2$. Replacement of the first three (approximately) equal signs in Eqs. (24) by greater-than signs restricts the region of possible root locations in the s plane,

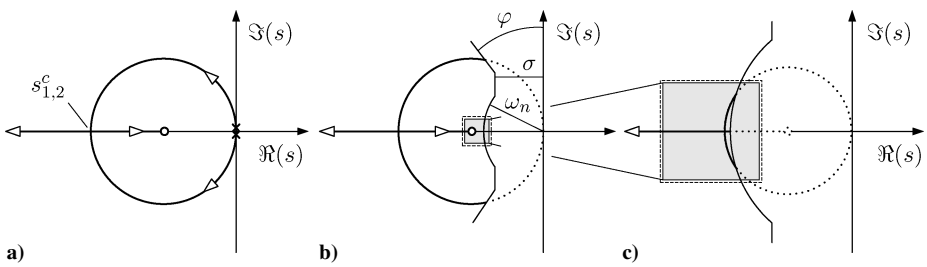

Fig. 5 Linear controller gain selection using root-locus method.

as shown in Fig. 5b. Because we are aiming for a critically damped system, it is preferable to choose c (and therefore K or a) as small as possible to minimize the control input (thrust) without violating the performance constraints (Fig. 5c). Note that, for a critically damped system, the overshoot $M_p = 0$ by definition. Therefore, in Eqs. (24), $\zeta = 1$, and so $\varphi = \pi/2$.

In the following section the performance of the control law is discussed.

Examples

We developed and implemented a generic simulation code to validate the performance of the control laws presented in the preceding sections. In particular, the mission scenarios described earlier were used to define desired trajectories. System and simulation parameters are listed in Table 1. For the perturbed initial conditions response simulation, the perturbation vectors were generated randomly with an upper bound of $\delta x/x \leq 10^{-3}$ for each element of the vectors. Finally, the initial and final radial distance of the point masses for mission scenarios 2 and 3 were chosen to be $R_0 = r_{0_+} = 10$ m and $R_f = r_{0_-} = 30$ m.

Figures 2–4 show simulation results for the various mission scenarios. The initial conditions perturbation response is illustrated in Fig. 2. The randomly disturbed TSS approaches the relative equilibrium motion with a steady-state radial distance of the point masses of $r^e = 10$ m, within a period of about 5.0 s. During this process, the thrust requirements in the radial direction are significantly lower than they are in the azimuthal direction, which is in part due to the effect of the tethers.

The results for mission scenario 2 are shown in Fig. 3. The tether length control law is a simple linear and constant relationship between the radial distance of the point masses and the unstrained tether lengths. As a result, during deployment/retrieval of the tethers, the overall tether tension decreases/increases relatively, which, in turn, requires increasing/decreasing thrust levels. The mission duration is approximately 900 s, and the position errors for this particular setup are all in the centimeter range. Required controls in the r and θ directions range up to 15 N and 20 Nm, respectively. This particular case also shows that the choice of the constant relating the unstrained tether length to the actual particle-to-particle distance is suboptimal. The direction of the radial control component remains negative during the mission, and the system steadily diverges from a possible state of a relative equilibrium during deployment.

Because such a simple mission trajectory does not guarantee time efficient and complete coverage of the observational plane, we introduced the more natural Archimedes spiral pattern as the desired trajectory in an earlier section. Also, a more complex tether length control law is used to minimize radial control effort. By the use of Eq. (10), the unstrained tether length is chosen to keep the TSS in a state corresponding to an instantaneous relative equilibrium at all times during the entire mission. Furthermore, for this scenario, we also include smoothing functions with a duration of 40.0 s each to decrease the radial control peaks observed in Fig. 3. Simulation results are illustrated in Fig. 4. The specific tether length control law significantly decreases required control input in the radial direction during the entire mission. The use of smoothing functions reduces peak control input in the radial and angular direction during transition times. Also note that the radial error is reduced by about four orders of magnitude. Similar to the earlier presented mission scenarios, the control of the angular direction requires the bigger part of the overall control effort.

Table 1 System and simulation parameters

Parameter	Variable
Point masses m_i, kg	50.0
Mirror diameters D_i, m	variable
Young's moduli E_{ij}, N/mm^2	10,000
Tether cross sections A_{ij}, mm^2	0.79
Damping parameters a_{ij}, s	0.0
Initial radial distance R_0, m	10.0
Final radial distance R_f, m	variable
Integration time step dt, s	0.02
IC disturbances $\delta x_{i,j}/x_{i,j}$	$\leq 10^{-3}$
Rise time (step response) t_r, s	2.0
Settling time (step response) t_s, s	5.0
Overshoot (step response) M_p, %	0.0
Control parameters $\alpha_{i,1}$, $[\alpha_{i,1}]$	2.0
Control parameters $\alpha_{i,0}$, $[\alpha_{i,0}]$	1.0

In all of the cases presented, the magnitude of the angular momentum vector undergoes significant changes during tether deployment/retrieval phases. For mission scenario 2, $\dot{\theta}_{i,d}$ and $\dot{r}_{i,d}$ are constant. Temporarily dropping index notation, we see that with $h = \|\boldsymbol{h}\| \propto \dot{\theta}_{i,d} r^2$, the change in angular momentum is $(\mathrm{d}/\mathrm{d}t)h \propto r$, and the control force is linearly increasing during tether deployment and linearly decreasing during tether retrieval. In the case of mission scenario 3 the tangential velocity of the point masses $v = v_{\max}$ is constant and $r \propto \sqrt{(t + c_2)}$. Therefore, with $h \propto vr$ it is straightforward to show that $\dot{h} \propto \dot{r} \propto 1/\sqrt{(t + c_2)}$.

We point out that for the current analysis, the control power required to enforce the tether length/tension law has not been taken into account. This issue will have to be addressed to make objective judgements on the performance of the control system.

Parameter Dependence of Total Required Control Impulse

In this section, we study the parameter dependence of the total required control impulse for mission scenario 3. Similar to the examples discussed earlier, we are interested in the performance of the symmetric triangular TSS. For this reason, any parameter variation is conducted in a symmetric fashion, for example, the mirror diameters D_i of all three mirrors are equal ($D_i = D$). The parameters of interest are Young's modulus of the tethers, $E_{ij} = E$, the mirror diameter, $D_i = D$, the final radial distance of the point masses from the center of mass of the TSS, R_f, and the desired tangential velocity of the point masses, $v = v_{\max}$. Before presenting simulation results, we propose a mathematical model for the total required control impulse as a function of the aforementioned system parameters to facilitate subsequent discussion.

Mathematical Model for Total Required Control Impulse

The overall required control impulse to complete mission scenario 3 for a particular set of system parameters can be divided into two parts. The first major contribution to the required control impulse is applied in the angular direction and regulates the angular momentum of the TSS according to the desired trajectory. As shown in the preceding section, the angular momentum undergoes significant changes during deployment and retrieval of the tethers. The second control part is a radial control component that significantly contributes to the overall control effort during periods of time when the TSS is in a transitional phase between steady spin and deployment/retrieval of the tethers and vice versa. Other contributions to the overall control effort, such as damping terms to account for longitudinal tether vibrations, are negligible, mainly due to the smoothness of the desired trajectory. When index notation due to system and parameter symmetry is dropped, the time rate of change of the angular momentum for mission scenario 3 is

$$\dot{h} = 3mv\dot{r} \equiv 3u_{\theta_\pm} r \tag{25}$$

where $u_{\theta_\pm}$ is the control input in angular direction. As defined in Eqs. (14), where $\pm$ appears in an equation or as part of a variable name, the upper sign denotes tether deployment, and the lower sign denotes tether retrieval. By the use of Eqs. (15), the angular control input can be rewritten as

$$u_{\theta_\pm} = \frac{\pm mv\alpha}{r_{0_\pm}^2 \pm 2\alpha\left(t - t_{0_\pm}\right)} = \frac{\pm 3Dmv^2}{2\pi\left[r_{0_\pm}^2 \pm 3Dv\left(t - t_{0_\pm}\right)/\pi\right]} \tag{26}$$

Integration of Eqs. (26) over a tether deployment or retrieval process yields, for the control impulse,

$$\Upsilon_{\theta_\pm} = \int_{t_{0_\pm}}^{t_{f_\pm}} \frac{\pm mv/2}{2\pi r_{0_\pm}^2 \big/ (6Dv) \pm \left(t - t_{0_\pm}\right)}\,\mathrm{d}t$$

$$= \frac{mv}{2}\,\ell_n\left[\frac{2\pi r_{0_\pm}^2}{6Dv} \pm \left(t - t_{0_\pm}\right)\right]\Bigg|_{t_{0_\pm}}^{t_{f_\pm}} \tag{27}$$

From Eqs. (15), we see that the tether deployment and retrieval times can be obtained as $t_{f_\pm} = \pi(\pm r_{f_\pm}^2 \mp r_{0_\pm}^2)/(3Dv) + t_{0_\pm}$. After substitution of this expression into Eq. (27), the angular control impulse results:

$$\Upsilon_{\theta_\pm} = \frac{mv}{2}\,\ell_n\left[\frac{2\pi r_{0_\pm}^2 \pm 2\pi\left(\pm r_{f_\pm}^2 \mp r_{0_\pm}^2\right)}{2\pi r_{0_\pm}^2}\right]$$

$$= mv\,\ell_n\left(\frac{r_{f_\pm}}{r_{0_\pm}}\right) = \pm mv\,\ell_n\left(\frac{R_f}{R_0}\right) \tag{28}$$

which shows that $\Upsilon_{\theta_\pm}$ is independent of the mirror diameter. It is apparent from Eq. (26) that the angular control force depends on the mirror diameter. Especially for small $(t - t_{0_\pm})$, that is $(t - t_{0_\pm}) < (\pi r_{0_\pm}^2)/(3Dv)$, u_θ is approximately proportional to the mirror diameter. However, when the control force is integrated along the desired mission trajectory, this increase in control force $(u_\theta \propto D)$ is compensated by a reduced mission duration, $(t_{f_\pm} - t_{0_\pm}) \propto 1/D$.

The control effort in the radial direction is derived in a similar fashion. As mentioned before, the radial control component contributes significantly to the overall control effort when the TSS is in a transitional phase, that is, $t_s^o < t < t_s^f$. By interpretation of R_0 and R_f in Eq. (28) as the radial distances at the initial and terminal points of the smoothing phase, the radial control effort for a tether deployment or retrieval process can be written as

$$\Upsilon_{r_\pm} = \pm mv\left\{\ell_n\left(\frac{\sqrt{R_0^2 + \alpha\Delta t_s}}{R_0}\right) + \ell_n\left(\frac{R_f}{\sqrt{R_f^2 - \alpha\Delta t_s}}\right)\right\} \tag{29}$$

where $\Delta t_s = t_s^f - t_s^i$, and where we choose $t^\star - t_s^o = t_s^f - t^\star = \Delta t_s/2$ for all smoothing processes for convenience. With Eqs. (28) and (29), the overall control impulse for the three point masses to complete mission scenario 3 becomes

$$\Upsilon(R_f, D, v) = 3\left(2\left|\Upsilon_{\theta_\pm}\right| + 2\left|\Upsilon_{r_\pm}\right|\right) = 6mv\,\ell_n\left(\frac{R_f^2\sqrt{R_0^2 + \alpha\Delta t_s}}{R_0^2\sqrt{R_f^2 - \alpha\Delta t_s}}\right) \tag{30}$$

with $\alpha = 3Dv/2\pi$. We note that in Eq. (30), the parameters R_f, $\alpha = \alpha(D, v)$, and Δt_s cannot be chosen independently. In particular, to obtain a smooth trajectory, the times t_s^o and t_s^f for each smoothing process have to be chosen such that one process is completed before the ensuing one begins. For our simulations, we use $\Delta t_s/2 = 20$ s. This choice introduces a constraint for the parameters R_f and α of the form

$$t_f - t_0 = \frac{R_f^2 - R_0^2}{2\alpha} = \frac{\pi\left(R_f^2 - R_0^2\right)}{3Dv} \geq \Delta t_s = 40\ \text{s} \tag{31}$$

We point out that this constraint is unlikely to be violated for a SPECS mission with typical tether deployment and retrieval periods in the order 10^5 s for a 1-km baseline interferometer.

Comparison of Simulation Results and Analytic Estimates

The mathematical model derived in the preceding paragraph is interesting in many respects. According to Eq. (28), a change in mirror diameter does not affect the angular control input that regulates the total angular momentum of the system. Hence, for the particular desired trajectory used, an Archimedes spiral, the resulting control effort equals what we would intuitively expect when simply applying a basic law of physics, namely, the conservation of angular momentum: The total angular control input (which is, in effect, a control torque) is equal to the change in angular momentum. Clearly, the change in angular momentum is a function of R_0, R_f, and v, only (for given masses m_i). Another interesting result is that the radial and, therefore, also the total required control impulse are both uniformly increasing functions of mirror diameter and tangential tracking velocity. An increase in the mirror diameter or the tangential velocity increases the initial time derivative of the radial distance [Eq. (13)] during tether deployment, which can be accomplished only by an increased radial control input. Similar arguments can be used to explain an increased radial control effort during the final stages of the tether deployment.

Figures 6–9 show the total required control impulse as a function of one continuous parameter for a selection of discrete values of the other parameter. Data points obtained from simulations are denoted by plus signs, and the bold lines mark the analytic estimate gathered by the use of Eq. (30). As expected, the total control impulse increases uniformly with R_f, D, and v. In the preceding section, we noted that the parameters R_f, $\alpha = \alpha(D, v)$, and Δt_s cannot be chosen independently. For example, for the data point in Fig. 8 where $R_f = 20.0$ m and $v = 2.7$ m/s, the tether deployment time is $t_f - t_0 = 23.27\ \text{s} < \Delta t_s = 40$ s. Therefore, the constraint (31) is violated, and a smooth trajectory cannot be obtained. The additional control effort to account for this nonsmoothness dramatically increases the overall required control impulse. In general, the simulation results compare well to the analytic expression, except for those parameter sets where the desired trajectory becomes nonsmooth (generally for small R_f and large D and/or v). The effect of nonsmooth trajectories was not considered in the derivation of the mathematical model, and so this result is expected.

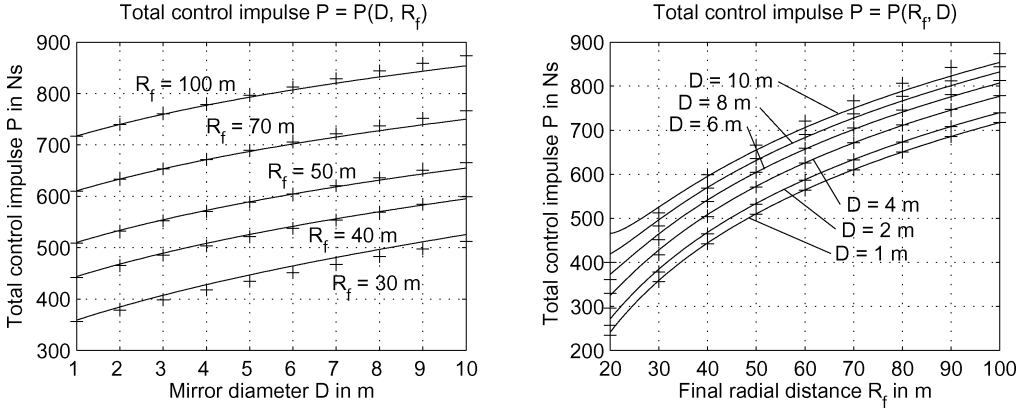

Fig. 6 Estimate for total control impulse P for tangential velocity $v_{\max} = 1$ m/s.

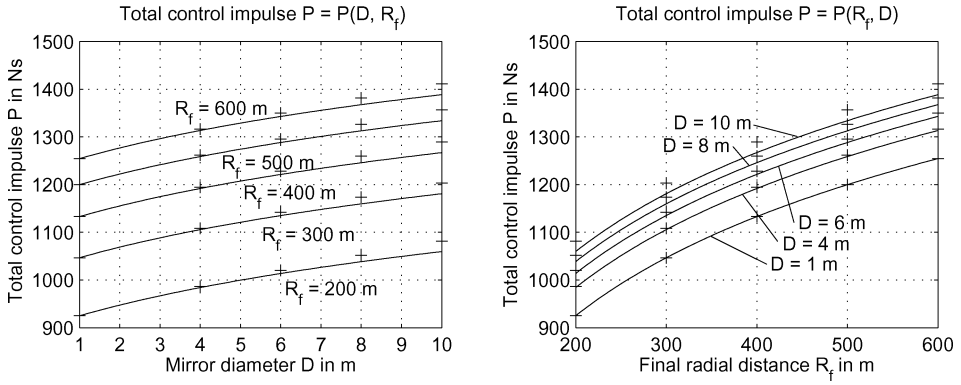

Fig. 7 Estimate for total control impulse P for tangential velocity $v_{max} = 1$ m/s.

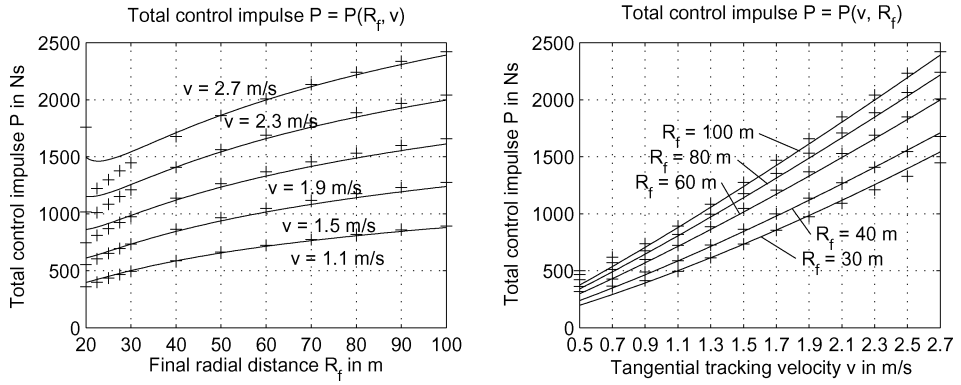

Fig. 8 Estimate for total control impulse P for mirror diameter $D = 5$ m.

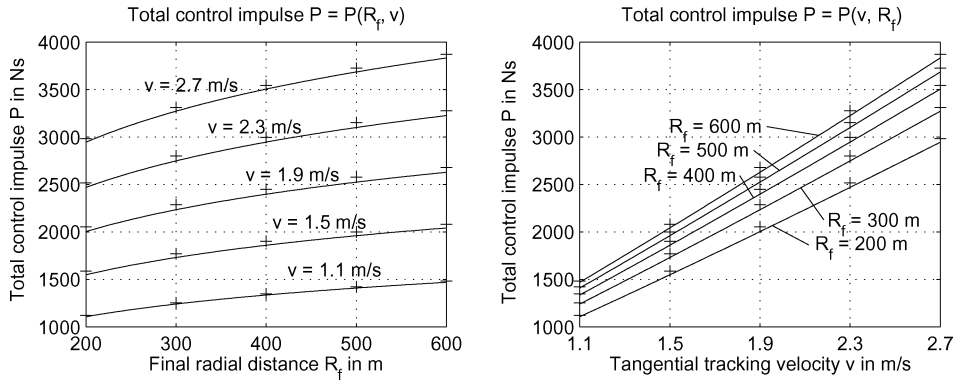

Fig. 9 Estimate for total control impulse P for mirror diameter $D = 5$ m.

Conclusions

Techniques to control the motion of a TSS comprising n point masses and interconnected by m idealized tethers are presented. Specifically, the control problem of a triangular and symmetrical TSS with $n = 3$ point masses and $m = 3$ tethers is considered. Several mission scenarios for an example mission are introduced, and asymptotic tracking laws based on input-state feedback linearization are developed. Implementation of smooth mission trajectories is essential to guarantee satisfactory control performance. Required thrust levels can be further decreased by the use of a tether length control law that keeps the system in an instantaneous relative equilibrium during the entire mission. However, the discontinuous character of the tether elastic forces, for example, transition between taut/slack tether) introduces issues related to the application of the particular control technique used. A mathematical model to estimate the overall required control impulse is presented and is shown to compare well with simulation results. This model provides a means to predict the influence of system parameters on the total control input.

Acknowledgments

This work was supported by David Quinn of NASA Goddard Space Flight Center and by Arje Nachman of the U.S. Air Force Office of Scientific Research.

References

[1]Johnson, L., Glichrist, B., Estes, R. D., and Lorenzini, E., "Overview of Future NASA Tether Applications," *Advances in Space Research*, Vol. 24, No. 4, 1999, pp. 1055–1063.

[2]Maccone, C., "Tethered System to Get Magnified Radio Pictures of the Galactic Center From a Distance of 550 AU," *Acta Astronautica*, Vol. 45, No. 2, 1999, pp. 109–114.

[3]Quadrelli, M. B., Hadaegh, F. Y., Lorenzini, E. C., and Bombardelli, C., "Precision Tethered Formations for LEO and Space Interferometry

Applications," *16th International Symposium on Space Flight Dynamics*, California Inst. of Technology, Jet Propulsion Lab., Pasadena, CA, 2001.

[4]Cosmo, M., and Lorenzini, E., *Tethers in Space Handbook*, 3rd ed., prepared for NASA/Marshall Space Flight Center (MSFC) by Smithsonian Astrophysical Observatory, Cambridge, MA, 1997, pp. 1–35.

[5]Beletsky, V. V., and Levin, E. M., *Dynamics of Space Tether Systems*, Advances in Astronautical Sciences, Vol. 83, Univelt, San Diego, CA, 1993, pp. 20–33.

[6]Quinn, D. A., and Folta, D. C., "A Tethered Formation Flying Concept for the SPECS Mission," *Proceedings of the 23rd Rocky Mountain Guidance and Control Conference*, Advances in the Astronautical Sciences, Vol. 104, Univelt, San Diego, CA, 2000, pp. 183–196.

[7]Kim, M., and Hall, C. D., "Lyapunov and Halo Orbits About L_2," *Proceedings of the 2001 AAS/AIAA Astrodynamics Specialist Conference*, Advances in the Astronautical Sciences, Vol. 109, Univelt, San Diego, CA, 2002, pp. 349–366.

[8]Decou, A. B., "Attitude and Tether Vibration Control in Spinning Tethered Triangles for Orbiting Interferometry," *Journal of the Astronautical Sciences*, Vol. 41, No. 3, 1993, pp. 373–398.

[9]Decou, A. B., "Tether Static Shape for Rotating Multimass, Multitether, Spacecraft for Triangle Michelson Interferometer," *Journal of Guidance, Control, and Dynamics*, Vol. 12, No. 2, 1989, pp. 273–275.

[10]Misra, A. K., "Equilibrium Configurations of Tethered Three-Body Systems and Their Stability," *Proceedings of the 2001 AAS/AIAA Space Flight Mechanics Meeting*, Advances in the Astronautical Sciences, Vol. 108, Univelt, San Diego, CA, 2001, pp. 1757–1772.

[11]Misra, A. K., Amier, Z. E., and Modi, V. J., "Attitude Dynamics of Three-Body Tethered Systems," *Acta Astronautica*, Vol. 17, No. 10, 1988, pp. 1059–1068.

[12]Misra, A. K., and Modi, V. J., "Three-Dimensional Dynamics and Control of Tether-Connected N-Body Systems," *Acta Astronautica*, Vol. 26, No. 2, 1992, pp. 77–84.

[13]Keshmiri, M., and Misra, A. K., "General Formulation for N-body Tethered Satellite System Dynamics," *Journal of Guidance, Control, and Dynamics*, Vol. 19, No. 1, 1996, pp. 75–83.

[14]Misra, A. K., Bellerose, J., and Modi, V. J., "Dynamics of a Tethered System Near the Earth–Moon Lagrangian Points," *Proceedings of the 2001 AAS/AIAA Astrodynamics Specialist Conference*, Advances in the Astronautical Sciences, Vol. 109, Univelt, San Diego, CA, 2002, pp. 415–435.

[15]Farquhar, R. W., "Tether Stabilization at a Collinear Libration Point," *Journal of the Astronautical Sciences*, Vol. 49, No. 1, 2001, pp. 91–106.

[16]Farquhar, R. W., "The Control and Use of Libration Point Satellites," Stanford Univ. Rept. SUDAAR–350, Dept. of Astronautics and Aeronautics, Stanford, CA, 1968, reprinted as NASA Technical Report TR R-346, 1970.

[17]Colombo, G., "The Stabilization of an Artificial Satellite at the Inferior Conjunction Point of the Earth–Moon System," Smithsonian Astrophysical Observatory Special Rept. 80, Cambridge, MA, Nov. 1961.

[18]Gates, S. S., "Multi-tethered Space-based Interferometers: Particle System Model," U.S. Naval Research Lab., Tech. Rept. NRL/MR/8231-01-8579, Washington, DC, Sept. 2001, pp. 1–32.

[19]Sepulchure, R., Janković, M., and Kokotović, P., *Constructive Nonlinear Control*, 1st ed., Springer-Verlag, London, 1997, pp. 287–295.

[20]Isidori, A., *Nonlinear Control Systems*, 3rd ed., Springer-Verlag, London, 1995, pp. 219–277.

[21]Kim, M., and Hall, C. D., "Dynamics and Control of Tethered Satellite Systems for NASA's SPECS Mission," *Proceedings of the 2003 AAS/AIAA Astrodynamics Specialist Conference*, Advances in the Astronautical Sciences (to be published).

[22]Sastry, S., *Nonlinear Systems*, Springer-Verlag, New York, 1999, pp. 384–440.

[23]Franklin, G. F., and Powell, J. D., *Feedback Control of Dynamic Systems*, 3rd ed., Electrical and Computer Engineering, Addison Wesley, Longman, Reading, MA, 1994, pp. 85–116.